

## Characterization of the $\text{Sc}_2\text{O}_3/\text{La}_2\text{O}_3$ High- $\kappa$ Gate Stack by STM

Y. C. Ong<sup>1</sup>, D. S. Ang<sup>1</sup>, S. J. O'Shea<sup>2</sup>, K. L. Pey<sup>1</sup>, T. Kawanago<sup>3</sup>, K. Kakushima<sup>3</sup>, H. Iwai<sup>3</sup>

<sup>1</sup>School of Electrical and Electronic Engineering, Nanyang Technological University, Singapore 639798 (E-Mail: [N040136@ntu.edu.sg](mailto:N040136@ntu.edu.sg))

<sup>2</sup>Institute of Material Research and Engineering, 3, Research Link, Singapore 117602

<sup>3</sup>Frontier Collaborative Research Center, Tokyo Institute of Technology, 4259 Nagatsuta, Midori-ku, Yokohama, 226-8502, Japan

### 1. Introduction

Lanthanum-based dielectrics have recently emerged as potential candidates for 0.5 nm equivalent oxide thickness scaling<sup>1</sup>. This work presents nanoscale current-voltage characteristics, via scanning tunneling microscopy (STM), of the  $\text{Sc}_2\text{O}_3/\text{La}_2\text{O}_3$  gate stack. Different types of localized leakage sites are clearly distinguished. Possible precursor sites for breakdown are identified with evidence from constant imaging tunneling spectroscopy (CITS).

### 2. Experimental

The bi-layer gate stack, consisting of 3 nm  $\text{Sc}_2\text{O}_3$  (top) and 4 nm  $\text{La}_2\text{O}_3$  on a p-Si substrate was prepared by electron-beam vapor deposition in ultra-high vacuum (UHV). Post-deposition anneal was done in nitrogen at 300 °C. The interfacial oxide layer is ~1 nm thick. An UHV scanning tunneling microscope was used to study the gate stack at nanometer spatial resolution. The biasing voltage  $V_s$  was applied to the substrate, and thus positive (negative)  $V_s$  corresponds to electron injection from the tip (substrate). STM images were obtained at a biasing condition of -4 V, 20 pA (bias set point); the tunneling current was maintained constant by a feedback circuit. The constant current image of the high- $\kappa$  gate stack contains information on both film morphology and electrical properties. To examine the electrical properties of the gate stack separately, CITS was acquired by measuring the tunneling spectrum at each pixel. The tunneling current at each pixel can be combined to form a current map of the scanned area at a given voltage.

### 3. Results and Discussion

#### A. Localized Leakage Sites

Fig 1 shows constant current and constant voltage images of the bi-layer gate stack. Based on the characteristics of the tunneling spectra (Fig. 2) in the positive  $V_s$  regime, 3 different localized leakage sites (labeled A, B and C) may be identified. The curve labeled as "Ref." in Fig. 2 is the average tunneling spectrum of all pixels in the 30 x 30 nm<sup>2</sup> image. Type A sites correspond to locations with tunneling spectrum shifted almost parallel to the Ref. curve. The parallel shift towards less positive  $V_s$  implies an overall lowering of tunneling barrier at the tip/high- $\kappa$  interface<sup>2</sup>. In the constant voltage images (Fig. 1(c) and (d)), type A sites manifest as a bright shade at all positive  $V_s$  values. The tunneling spectrum of type B sites exhibit typical SILC characteristic, where increased tunneling current is observed only at low  $V_s$ . As  $V_s$  is increased, the tunneling current curve and the Ref. curve merge (Fig. 2). This observation implies that type B leakage sites arise from trap-assisted tunneling<sup>3</sup>. Hence, type B sites register as a bright shade only in Fig. 1(c) ( $V_s = +2.2$  V) but not in Fig. 1(d) ( $V_s = +4$  V). The tunneling spectrum of type C leakage sites, on the other hand, is lower (higher) than the Ref. curve for positive (negative)  $V_s$ . Type C sites thus appear to be active only in the negative  $V_s$  regime and register as a bright shade only in Fig. 1(b) ( $V_s = -2.2$  V).

#### B. Electrical Stress Induced Evolution

Fig. 3(a) presents a merger of constant voltage images at

$V_s = -2.3$  V,  $+2.3$  V, and  $+4$  V, showing type A and C leakage sites. Type B leakage sites are not observed within the scanned area. In a subsequent constant current imaging scan, the tip injection voltage was increased to  $+5$  V during tunneling spectrum measurements. Fig. 3(b) depicts the constant voltage image at  $V_s = +5$  V. An increase in the density of bright shades, particularly in the vicinity of the pre-existing type A leakage sites of Fig. 3(a), should be highlighted. Fig. 3(c) compares the tunneling spectra at the bright and normal shades in Fig. 3(b). Greater tunneling current at large positive  $V_s$  implies that the bright shades in Fig. 3(b) correspond to type A leakage sites. This observation shows that increased tip injection generates more type A leakage sites. Moreover, in Fig. 3(b), the absence of bright shades at locations corresponding to the type C leakage sites in Fig. 3(a) implies that certain pre-existing type C leakage sites did not evolve into type A leakage sites on applying  $+5$  V. Fig. 4(a) is a zoom-out 100 x 100 nm<sup>2</sup> constant current image showing a stressed region. Bright shades, which correspond to type C leakage sites, in the constant voltage ( $V_s = -2.2$  V) image of Fig. 4(b) spread fairly uniformly over the scanned area, with no particular increase in density within the stressed region. On the other hand, a concentration of bright shades, corresponding to type A leakage sites, within the stressed region is evident in the constant voltage image at  $V_s = +4$  V [Fig. 4(d)].

Similar results are obtained under increased substrate injection voltage, by starting  $V_s$  at  $-5$  V instead of  $-4$  V during tunneling spectrum measurement. The constant voltage image in Fig. 5(b) shows an increased concentration of bright shades in the vicinity of pre-existing type A leakage sites [Fig. 5(a)]. The uniform distribution of bright shades in the constant voltage image (Fig. 6(b)) further supports the inference that type C leakage sites are not affected by the increased substrate injection. As for tip injection, increased substrate injection increases significantly the density of type A leakage sites within the stressed region [Fig. 6(d)].

### 3. Summary

The  $\text{Sc}_2\text{O}_3/\text{La}_2\text{O}_3$  gate stack on p-Si was characterized using UHV STM. Three distinct localized leakage sites are observed. Type A leakage sites are characterized by an overall lowering of electron tunneling barrier, and are observed under both bias polarities. Type B leakage sites exhibit SILC characteristic, and are observed at low positive  $V_s$ , but not at negative  $V_s$ . Type C leakage sites are observed under negative  $V_s$  but exhibit lower current than the average background tunneling current under positive  $V_s$ . Type A leakage sites are shown to be the main contributor to leakage degradation under increased tip and substrate injection.

### References

- [1] Wu *et al.*, *IEEE Electron Dev. Lett.*, vol. 21, pp. 341-343, 2000.
- [2] Carim *et al.* *Science*, vol. 237, pp. 630, 1987
- [3] Seko *et al.* *Jpn. J. Appl. Phys.*, vol. 45, pp. 2954, 2006.

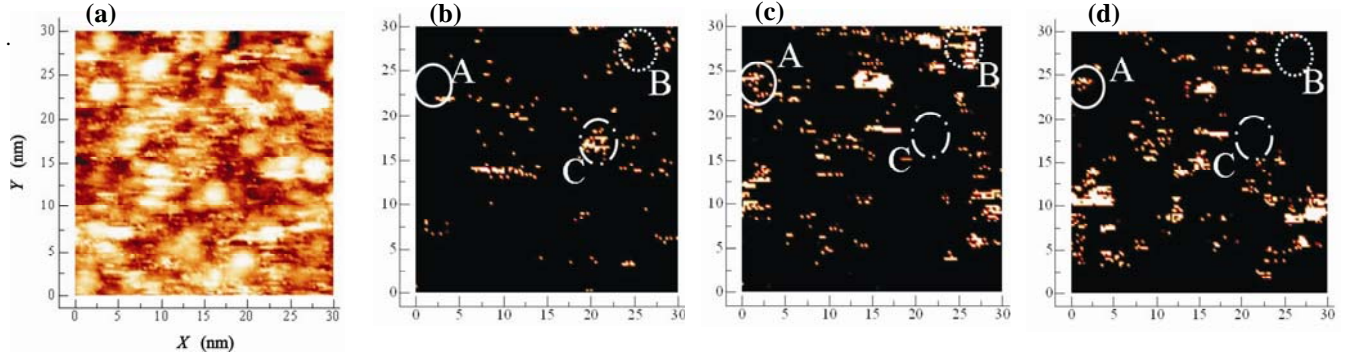


Fig. 1 (a) Constant current STM image of a  $\text{Sc}_2\text{O}_3/\text{La}_2\text{O}_3$  gate stack; bias set point:  $V_s = -4$  V,  $I = 20$  pA. To separate the electrical property variation from surface morphology, constant voltage images are constructed from the tunneling spectrum measured at each pixel in (a). (b) Constant voltage image (CVI) at  $V_s = -2.2$  V showing presence of type C but not A and B leakage sites. (c) Constant voltage image at  $V_s = +2.2$  V showing type A and B but not C leakage sites. (d) Constant voltage image at  $V_s = +4$  V showing only type A leakage sites. For the CVI, only the upper-tail end of the current distribution is plotted.

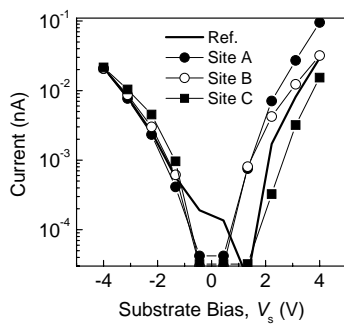


Fig. 2 Tunneling spectra of type A, B and C leakage sites, showing distinct differences in the positive  $V_s$  regime. Marginal difference among the tunneling spectra in the negative  $V_s$  regime due to vacuum gap correction caused by bias set point ( $-4$  V,  $20$  pA).

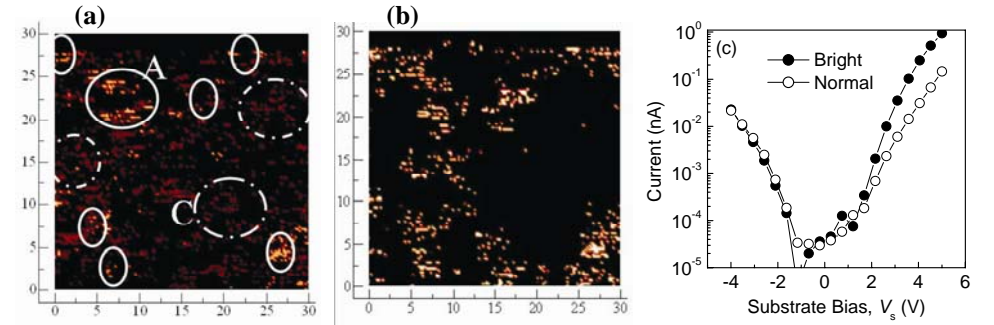


Fig. 3 (a) Merged constant voltage image for  $V_s = -2.3$ ,  $+2.3$  and  $+4$  V, showing presence of only type A (solid lines) and C (dash-dot lines) leakage sites. (b) Constant voltage image at  $V_s = +5$  V, showing an increased density of bright shades in the vicinity of type A leakage sites. Type C leakage sites, which are observed in (a) at  $V_s = -2.3$  V are not observed in (b). (c) Averaged tunneling spectra of bright and normal shades in (b).

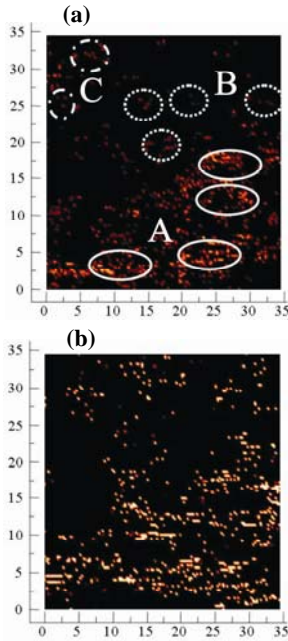


Fig. 5 (a) Merged constant voltage image for  $V_s = -3.2$ ,  $+2.2$  and  $+4$  V. (b) Constant voltage image at  $V_s = -5$  V, showing an increased density of bright shades in the vicinity of type A leakage sites.

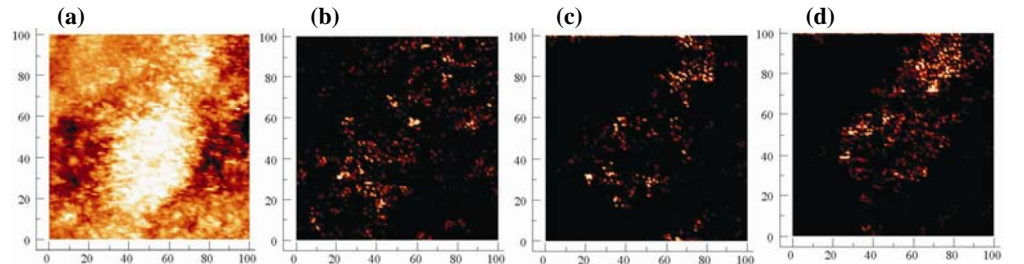


Fig. 4 (a) Zoom-out constant current image; bias set point:  $V_s = -4$  V,  $I = 20$  pA. The scanned area in Fig. 3 appears as a bright shade. Constant voltage image; (b)  $V_s = -2.2$  V; (c)  $V_s = +2.2$  V; (d)  $V_s = +4$  V.

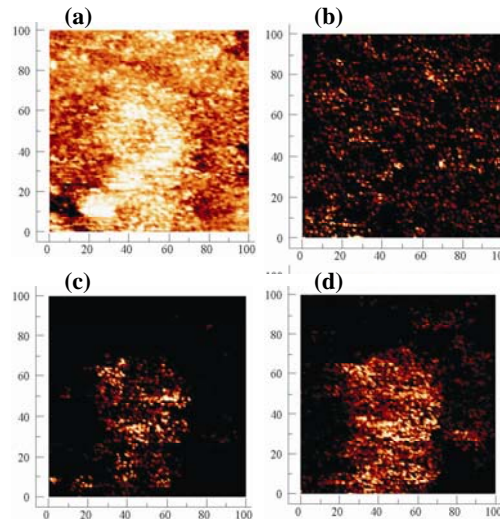


Fig. 6 (a) Zoom-out constant current image; bias set point:  $V_s = -4$  V,  $I = 20$  pA. The scanned area in Fig. 5 appears as a bright shade. Constant voltage image at; (b)  $V_s = -2.2$  V showing a fairly uniform distribution of type C leakage sites over the zoom-out area, with no particular increase in the scanned area which receives increased substrate injection; (c)  $V_s = +2.2$  V; (d)  $V_s = +4$  V showing a high concentration of bright shades corresponding to type A leakage sites within the scanned area.